Structure and activity of a functional derivative of *Clostridium botulinum* neurotoxin B*

Geoffrey Masuyer[1], Matthew Beard[2], Verity A. Cadd[2], John A. Chaddock[2] and K. Ravi Acharya[1,3]

[1]Department of Biology and Biochemistry, University of Bath, Claverton Down, Bath BA2 7AY, United Kingdom

[2]Syntaxin Limited, Units 4-10, The Quadrant, Barton Lane, Abingdon, Oxon OX14 3YS, United Kingdom

[3]To whom correspondence may be addressed: Department of Biology and Biochemistry, Building 4 South, University of Bath, Claverton Down, Bath BA2 7AY, UK. Tel.: 44-1225-386238; Fax: 44-1225-386779; E-mail: bsskra@bath.ac.uk

ABSTRACT

Botulinum neurotoxins (BoNTs) cause flaccid paralysis by inhibiting neurotransmission at cholinergic nerve terminals. BoNTs consist of three essential domains for toxicity: the cell binding domain (Hc), the translocation domain (Hn) and the catalytic domain (LC). A functional derivative (LHn) of the parent neurotoxin B composed of Hn and LC domains was recombinantly produced and characterised. LHn/B crystallographic structure at 2.8Å resolution is reported. The catalytic activity of LHn/B towards recombinant human VAMP was analysed by substrate cleavage assay and showed a higher specificity for VAMP-1,-2 compared to VAMP-3. LHn/B also showed measurable activity in living spinal cord neurons. Despite lacking the Hc (cell-targeting) domain, LHn/B retained the capacity to internalize and cleave intracellular VAMP-1 and -2 when added to the cells at high concentration. These activities of the LHn/B fragment demonstrate the utility of engineered botulinum neurotoxin fragments as analytical tools to study the mechanisms of action of BoNT neurotoxins and of SNARE proteins.

Keywords: Botulinum neurotoxin, Protein engineering, SNARE, Crystal structure

INTRODUCTION

Botulinum neurotoxins (BoNTs) modulate cholinergic nerve terminals to cause a severe fatal illness, botulism. They are the most potent known protein toxins. There are seven serotypically distinct forms of BoNT, labelled A-G, expressed by various *Clostridium* strains. They are composed of a 150 kDa di-chain molecule that follows the AB bacterial toxin motif with intracellular targets. Upon binding and internalisation in neuronal cells the toxin blocks neurotransmitter release, leading to flaccid paralysis and potentially death. Despite their high toxicity, various preparations of BoNTs are available commercially for the treatment of muscular overactivity where at safe doses they can be used as therapeutic and cosmetic agents (Barnes et al., 2007; Moore et al., 2007).

BoNTs are synthesised as single polypeptides cleaved by clostridial or host proteases to its active form. The C-terminal heavy chain composes the binding (Hc) and translocation (Hn) domains of 50 kDa each, and is linked by a single disulfide bridge to the catalytic light chain (LC), a zinc endopeptidase. A loop from Hn wraps around the LC. The loop is called the belt region and is common to all BoNTs for which structural information is available. It is believed to play an essential chaperone role in the molecules' toxicity (Brünger et al., 2007; Galloux et al., 2008). BoNTs bind specifically to the nerve terminals and are endocytosed into a vesicle where the acidic environment provokes conformational changes. This allows the Hn domain to mediate translocation of LC via pore formation across the endosomal membrane into the cytosol (Koriazova and Montal, 2003; Fischer et al., 2007). The protease domain is then free to cleave one of the soluble *N*-ethyl-maleimide-sensitive fusion protein attachment receptor (SNARE) proteins. These proteins form a complex essential in the docking and fusion of synaptic vesicle (Sudhof et al., 2009).

Impairing the function of the SNARE complex causes inhibition of neurotransmission and hence paralysis.

The proteolytic activity of each BoNT serotype targets one of the SNARE proteins at a distinct site. BoNT/A and E cleave the pre-synaptic membrane protein SNAP-25 (synaptosomal associated protein of 25 kDa), whereas serotypes B, D, F and G are responsible for the cleavage of the vesicle associated membrane protein (VAMP), also known as synaptobrevin and cellubrevin. Unlike the other serotypes BoNT/C can proteolyse two SNARE proteins, both SNAP-25 and syntaxin. Substrate recognition has been a point of attention since it relies on an extended set of exosites located downstream and upstream of the scissile bond (Breidenbach and Brünger, 2004; Chen et al., 2007, 2008; Sikorra et al., 2008; Agarwal et al., 2009). Crystallographic evidence of SNAP-25 bound to LC/A highlighted this complex interaction with the substrate wrapping around LC (Breidenbach and Brünger, 2004). More recently, several mutation and kinetic studies with VAMP-2 illustrated the important regions for proteolysis of the VAMP specific Clostridial toxins (Chen et al., 2008; Sikorra et al., 2008). Alongside the structure of LC/F in complex with peptide inhibitors (Agarwal et al., 2009), this suggests a common mode of an extended substrate binding, each presenting with a different set of enzyme-substrate interactions.

Trypsinization of BoNT/A led to the discovery of an active fragment composed of the LC and Hn domains only, termed LHn/A (Shone et al., 1985). This fragment was later recombinantly expressed and showed catalytic properties similar to the parent toxin. This fragment was active on cells when added at high concentration (Chaddock et al., 2002). A more recent study again confirmed the ability of LHn/A to become internalized and act on the intracellular substrate despite lacking the binding domain (Hc) (Fischer et al., 2008). Furthermore, the crystal structure of LHn/A demonstrated that the structures of LC and Hn

are not destabilized by deletion of the Hc domain. This makes these proteins attractive candidates as scaffolds for the design of novel biological therapeutics (Chaddock and Marks, 2006; Foster, 2009; Masuyer et al., 2009).

Crystal structures of the full length BoNT/A (Lacy et al., 1998), B (Swaminathan and Eswaramoorthy, 2000), and E (Kumaran et al., 2009) have been determined, along with the LC of all serotypes (Agarwal et al., 2004, 2005; Segelke et al., 2004; Arndt et al., 2005, 2006; Jin et al., 2007). All the holotoxin structures available present single domains with similar folds. Nevertheless, inter-domain contacts were different in the E serotype compared to serotypes A and B. This indicates that BoNTs may be structurally more diverse than expected. A further illustration of this is the belt region from the Hn domain, for which limited information is available. Even though Hn is highly conserved between serotypes, the belt presents the most variation in primary sequence (Lacy and Stevens, 1999). Indications given from the holotoxin structures have highlighted the essential functional role it may play, and also proved useful in giving clues on substrate binding (Breidenbach and Brünger, 2004). In this context, LHn fragments represent a useful tool to further investigate the flexibility of the BoNT molecules in giving essential information on the interaction between the functional Hn and LC domains.

Here we report the crystal structure of the LHn fragment from serotype B botulinum neurotoxin at 2.8 Å. It demonstrates the stability of the translocation domain in association with the catalytic light chain. The metalloprotease activity of the parent toxin is conserved and presents differences in VAMP substrate specificity. If applied at suitably high concentrations, this active protease can be translocated inside neuronal cells despite the lack of a specific binding domain. It confirms the relevance of LHn/B as a functional

molecule and highlights the use of LHn as a tool for deciphering the mechanism of botulinum neurotoxin's action.

MATERIALS AND METHODS

LHn/B cloning, expression and purification – The synthetic gene encoding 880 amino acids of LHn/B was cloned into modified pET vector (Novagen, UK) with a C-terminal 6 x His-tag and transformed into *E. coli* BL21 expression cells. The LHn/B gene was engineered to encode for Factor Xa cleavage site (IEGR) between the LC and Hn domain between positions 449-452. Expression cultures of LHn/B were grown in 1L terrific broth at 220 rpm, 37°C until OD600 reads 0.5-0.6. Then cultures were incubated at 16°C and induced with IPTG (1mM). Cells were harvested after 18 h, and stored at -80°C until further use.

Cells were resuspended in 50 mM HEPES, pH 7.2, 0.2 M NaCl (buffer A) and lysed at 20,000 psi with a homogenizer (Constant Systems Ltd). Lysate was centrifuged for 45 minutes at 12,000 rpm. Soluble fraction was loaded onto a Ni^{2+}-charged chelating sepharose column (GE Healthcare). LHn/B eluted at 100 mM imidazole (dissolved in buffer A) and dialysed overnight at 4°C against buffer A. Activation of purified LHn/B is achieved by Factor Xa (New England BioLabs) treatment. The cleaved fusion protein was supplemented with ammonium sulfate to 1 M and loaded onto a Toyopearl Phenyl-350M column, equilibrated with 50 mM HEPES, pH 7.2, 1.0 M ammonium sulfate. LHn/B eluted at 0.7 M ammonium sulfate (in buffer) and dialysed overnight against buffer A at 4°C. The sample was finally concentrated using Vivaspin 50000 MWCO concentrator to 9 mg/mL and stored at -20°C. All concentrations were determined by A280 measurement.

Crystallization and structure determination – Crystals were grown in 15% PEG3350, 0.1 M BisTrisPropane pH 6.5, 0.2 M sodium sulfate. Diffraction data were collected at the Diamond Light Source, UK, beamline IO3. A complete dataset to 2.8 Å was collected from a single crystal at 100K (25% glycerol as cryoprotectant) using a Quantum-4 CCD detector (ADSC Systems, CA). The data were processed and scaled in orthorhombic space group $P2_12_12$ using MOSFLM and SCALA (CCP4, 1994; Leslie, 2006) (Table 1). Initial phases were obtained by molecular replacement using PHASER (McCoy et al., 2007) with the coordinates of a model based on the LHn fragment of the BoNT/B structure (PDB code 1EPW, Swaminathan and Eswaramoorthy, 2000). Crystallographic refinement was carried out using REFMAC5 (version 5.5) (Vagin et al., 2004). Manual adjustments and model fitting was done using COOT (version 0.6.1) (Emsley and Cowtan, 2004). Water molecules were added at positions where F_o–F_c electron density peaks exceeded 3σ and potential H-bonds could be made. The structure was validated using MOLPROBITY (Davis et al., 2007). Structure figures were drawn with PyMOL (DeLano Scientific LLC).

Enzymatic assay – LHn/B and BoNT/B (Metabiologics, US) were diluted to 0.1 μg/ml in buffer containing 50 mM HEPES pH 7.2, 20 μM $ZnCl_2$, 1 μg/μl BSA, 10 mM DTT, and incubated at 37°C for 30 minutes. Recombinant VAMP-1 (2-96), -2 (1-94) and -3 (2-77) substrates were expressed with a C-terminal GFP tag and purified. VAMP-GFP substrates were serial diluted and incubated with the test enzyme at 37°C for 1 hour. Reactions were stopped by adding 2x reducing sample buffer. Samples were then loaded on to a 4-12 % Bis-Tris gel (Invitrogen) along with BSA standards and visualized by staining with Simply Blue Safestain (Invitrogen). Assay results were quantified by densitometry (Syngene Bioimaging).

Embryonic spinal cord neuron (eSCN) assay – Spinal cords dissected from 14–15 day old foetal Sprague Dawley rats were cultured for 21 days using a modification of previously described method (Chaddock et al., 2002). eSCN were treated with serial dilutions of LHn/B and BoNT/B, and incubated at 37 °C with 10% CO_2 for 24 hours. Cells were lysed by removing all media and adding sample buffer (25% NuPAGE buffer, 10 mM DTT). After 20 minutes, samples were transferred into microcentrifuge tubes and heated at 95°C for 5 minutes. All samples were run on 12 % Bis-Tris gels (Invitrogen) and proteins were transferred onto nitrocellulose membranes (Invitrogen) using standard protocols. VAMP cleavage was monitored by measuring the disappearance of the specific VAMP immunoreactive bands compared to an internal control protein (GAPDH). Specific binding of VAMP-1, -2 and -3 primary antibodies (Abcam #ab3346, #ab3347 and #ab43080) was visualised using peroxidase-conjugated secondary antibodies and an enhanced chemiluminescent (ECL) detection system (Thermo), analysis was performed by densitometry (Syngene Bioimaging).

RESULTS AND DISCUSSION

Structure of LHn/B – The crystal structure of LHn/B has been determined at 2.8 Å resolution. The structure was refined to a final R_{free} = 28.2%, and R_{cryst} = 24.1% (Table 1, Fig. 1a), with 97.8% of amino acids in the Ramachandran plot allowed region.

The structure presents the two domains interacting tightly in a di-chain complex. The successful activation of LHn/B by Factor Xa at the engineered site was confirmed by SDS–PAGE analysis and the crystal structure, which shows a clear evidence of the cleavage by a break in electron density between LC and Hn (Suppl. Fig. S1). This region is

likely to be particularly important for BoNT activity and Hn-mediated delivery of LC in the cytosol. The resulting LC C-terminus and the disulfide bridge (A Cys 437– B Cys 461) between LC and Hn are stabilised through an anti-parallel β-sheet arrangement.

The overall structure of LHn/B (Fig. 1a) resembles BoNT/B without the binding domain, and superposition of LHn/B with its parent toxin gives an overall root mean square deviation of 0.95 Å for 837 C^{α}-atoms (Fig. 1b). The absence of the 50 kDa binding domain in LHn/B did not produce any major conformational change compared with the structure of full length BoNT/B.

LC is a metalloprotease with the catalytic zinc ion coordinated by the conserved tetrahedral arrangement of His 229, His 233, Glu 267 and a water molecule hydrogen bonded to Glu 230. While LC is fairly conserved among BoNTs, its activity is regulated by a complex substrate binding mechanism relying on dispersed exosites, away from the catalytic site, and in the case of BoNT/A the movement of flexible loop regions (Breidenbach and Brünger, 2004). The unstructured regions seen in LHn/B follow the same arrangements as seen in the full length toxin (Fig. 1). Residues 208-218, downstream of the active site, could not be modelled due to the lack of electron density. This may be the result of the loop's flexibility, even though the holotoxin structure shows it to be stabilised by interactions with helices α17 and α19 of Hn (Swaminathan and Eswaramoorthy, 2000).

Three long anti-parallel α–helices structure the Hn domain. The newly accessible solvent area left open by the lack of binding domain represents 1880 $Å^2$ and shows weak electrostatic potential (Suppl. Fig. S2). The interface between Hn and Hc of the holotoxin is based on 12 potential hydrogen bonds and some weaker van der Waals' contacts between loop 916-920 of Hc and helix α20 of Hn, as well as between the short linker helix of Hc

subdomains and loop 610-615 (Hn) (Swaminathan and Eswaramoorthy, 2000). The loop between residues 626-630 and the last 10 C-terminal residues (including the poly-His tag) of LHn/B could not be modelled due to lack of electron density. Strong inter-helical interactions allow Hn to keep its long helical conformation as illustrated by the perfect superposition of LHn/B with BoNT/B (Fig. 1b). The belt of Hn surrounding LC appears to be important for aspects of BoNT activity. The LHn/B structure demonstrates that the stability of this fold is based on strong interactions with LC and is similar to that seen in the holotoxin structure.

The crystallographic studies of LHn, serotypes A and B, highlight the exceptional structural stability of these fragments when compared to their parent holotoxins. LHn/A has been shown to conserve not only the structure, but also the catalytic property of BoNT/A, as well as a potential for intracellular activity (Chaddock et al., 2002; Fischer et al., 2008; Masuyer et al., 2009). Analysing the functionality of these fragments can therefore help understand the relationship between BoNT domains.

Proteolytic activity of LHn/B – The ability of LHn/B to retain its proteolytic activity was tested by looking at the cleavage of VAMP-1, -2 and -3. The three substrates were recombinantly produced as GFP-tagged constructs and were successfully hydrolysed by LHn/B (Fig. 2a). The cleavage site was checked for each substrate by N-terminal sequencing (Alta Bioscience, UK) and confirmed to be at the expected position, corresponding to the site of BoNT/B action (Fig. 2a).

A quantitative analysis of VAMP cleavage was performed by testing a range of different substrate concentrations at a fixed concentration of LHn/B (0.01 μg/ml). The plotted results were fitted according to a Michaelis-Menten equation. Substrate cleavage showed a higher maximal velocity (Vmax) for VAMP-1 and -2, (157±12 and 150±27

pmol/hour/μg enzyme respectively) than it did for VAMP-3 (27.9±3.5 pmol/hour/μg enzyme). Similar results were obtained with the BoNT/B control (unpublished results). A precise calculation of *Km* is difficult due to the nature of the assay, making the visualisation of low product levels hard to quantify. However determinations of *Km* only varied between 3.2 and 12 μM. It is likely that these apparent differences are within the errors of the estimations. Extensive work on the requirements for VAMP cleavage by Clostridial toxins have demonstrated that residues 60-87 of VAMP-2 were sufficient for efficient cleavage by BoNT, with residues within close distance of the scissile bond influencing the catalytic rate of reaction whereas several exosites on both sides of the bond were involved in binding (Chen et al., 2008). The primary sequences of the three VAMP tested (Fig. 2b) show that the scissile bond area is generally very conserved, apart for a minor difference at position P2 in VAMP-1 (VAMP-1/S – VAMP-2-3/T). This high degree of sequence conservation may explain the low variation in *Km* observed between the three substrates. The sequence alignment presents only one noticeable difference between VAMP-1 and -2 compared to VAMP-3 that lies near to the previously identified BoNT binding regions (VAMP-1-2/ Ala 39, 37 respectively compared to VAMP-3/ Asn 20). Further work is necessary to determine if this change accounts for the Vmax difference observed for these substrates. Another obvious difference in VAMP-3 compared to VAMP-1 and -2 is the N-terminal region which is considerably shorter and lacking the proline-rich region seen in VAMP-1 and -2. However, LC/B was proved to efficiently cleave a construct from VAMP-2 lacking residues 1-59 (Chen et al., 2008). The C-terminal transmembrane regions of the VAMP proteins were not included in these recombinant substrates. These regions were replaced by a GFP-tag and are unlikely to affect substrate binding.

Activity of LHn/B on spinal cord neurons – Studies with BoNT/A have shown that Hn is necessary for the transport of LC into cells (Koriazova and Montal, 2003). LHn/B is similarly composed of the catalytic light chain with its translocating partner domain. The function of Hn in absence of the BoNT binding domain was investigated on embryonic spinal cord neurons (eSCN) and compared to the holotoxin's effect. VAMP cleavage was monitored by Western blotting eSCN lysates after incubation with each protein. The blots were quantified by densitometry and the proportion of uncleaved VAMP remaining after treatment was plotted (Fig. 3).

The response followed dose-dependent sigmoidal curves for BoNT/B on VAMP-1 and -2, with sub-picomolar EC50. High concentrations of LHn/B also showed a sigmoidal dose-dependent response with EC50 of 15 and 170 nM on VAMP-2 and -1, respectively. This suggests that the binding domain of BoNT/B confers the toxin a more than 10^5-fold better efficiency in reaching its intracellular substrate. This is analogous to the phenomenon seen with BoNT/A and LHn/A where a 10^5 fold difference in concentration was observed on the inhibition of neurosecretion in similar cells (Chaddock et al., 2002). It is expected that intracellular VAMP cleavage observed here would also result in a similar inhibition of neurotransmission, thus representing a reliable model to assay VAMP-specific BoNTs.

The mechanism of entry of LHn/B into eSCN is unknown but is likely to rely on a non-specific process. Fisher et al. (2008) reported LHn/A's ability to translocate LC over a wide pH range compared to the native toxin, therefore increasing the likelihood of translocation. On the other hand, the possibility of a low affinity receptor for LHn/B in this cell type should not be excluded. The effect observed here is enhanced by the high LHn/B concentration and the sensitivity of the system used for testing. However, further

experimental evidence is required to fully understand the mechanism of internalization by the LHn molecule.

BoNT/B and LHn/B both showed higher apparent efficiency in cleaving VAMP-2 compared to VAMP-1 in eSCN (Fig. 3). However we do not fully understand the significance of this observation. Differences in the immunoreactivity, abundance and sub-cellular localization of these two SNAREs may play roles in accounting for this observation. VAMP-2 is known to be the most abundant protein in synaptic vesicles (Takamori et al., 2006). One possibility is that VAMP-2 might compete with VAMP-1 for binding to the LC. We also monitored VAMP-3 in treated eSCN lysates and did not detect any evidence for VAMP-3 cleavage (results not shown). The role of VAMP-3 (also called cellubrevin) has been previously investigated in non-neuronal cells using Clostridial tetanus toxin (McMahon et al., 1996). This report has highlighted its importance in the recycling of the plasma membrane, early endosome pathways, epithelial cell migration and adhesion (Proux-Gillardeaux et al., 2005). Despite VAMP-3 homology with VAMP-1 and -2 (Fig. 2b), there is no strong evidence for a direct role of VAMP-3 in neurosecretion. The lower specificity of LHn/B for this substrate demonstrated in the cell-free assay, along with the lack of intracellular proteolysis in eSCN, suggests that the toxin may have evolved to specifically target SNAREs directly mediating neurotransmission.

CONCLUSION

Botulinum neurotoxins are complex molecules that present a deadly machinery able to specifically inhibit synaptic transmission of cholinergic motorneurons. Each of the toxin's domains is essential for optimal potency and understanding their mechanism will allow to better harness this activity towards novel applications (Foster, 2009). New

approaches for the study of these molecules are required to determine the full extent of their potential. In the present study, the LHn/B fragment consisting the catalytic and translocation domains of BoNT/B, is shown to retain its native structure after deletion of the Hc domain. The functionality of the fragment was also demonstrated *in vitro* with its ability to cleave several VAMP substrates. Similar to wild type BoNT/B, LHn/B showed higher specificity for VAMP-1, and -2 compared to VAMP-3. Furthermore, LHn/B retained an ability to cleave intracellular VAMP in spinal cord neurons, indicating an intrinsic capacity of Hn to transport its catalytic partner within the cytosol. A detailed understanding of the processes involved in internalization and translocation into the cytoplasm is not yet available and requires further analysis, which may in turn give some indication on the translocation mechanism in the corresponding holotoxins.

LHn/B does not have the BoNT cell binding domain. The extent to which it can interact with and become internalized by other cell types represents an area for further study. This may reveal LHn/B as a useful pharmacological tool in the study of VAMP-mediated secretion events.

LHn fragments studied so far constitute stable soluble proteins that conserve the functionality of their parent holotoxin but lack the neuron specific targeting conferred by the binding domains of full-length BoNT. These fragments provide additional tools for understanding the structure-function relationship of BoNT domains in the intoxication process, and offer a new strategy for therapeutic and vaccine development (Chaddock and Marks, 2006). Determining the structure of other LHn serotypes will help refine our knowledge and explain the variations in activities seen between the botulinum neurotoxin serotypes.

Acknowledgements

We thank the scientists on beamline IO3 at Diamond Light Source (Oxon, UK) for their support during X-ray data collection.

Footnotes

*This work was supported by a post-graduate studentship to G.M. through a BBSRC-Syntaxin Limited (UK) CASE award and a Royal Society (UK) Industry Fellowship to K.R.A.

The atomic coordinates and structure factors (codes 2xhl and r2xhlsf) have been deposited in the Protein Data Bank, Research Collaboratory for Structural Bioinformatics, Rutgers University, New Brunswick, NJ (http://www.rcsb.org/)

Abbreviations used:

BoNT(/N), botulinum neurotoxin (/serotypes A-G); HC, heavy chain of BoNT; Hn, translocation domain of BoNT; LC, light chain of BoNT; LHn/N, light chain and translocation domain of BoNT serotypes (/A-G); SNAP-25, synaptosome-associated protein of 25kDa; SNARE, soluble N-ethyl-maleimide-sensitive factor attachment protein receptor; VAMP, vesicle associated membrane protein; GFP, green fluorescent protein; RMSD, root mean square deviation; eSCN, embryonic spinal cord neuron

FIGURE LEGENDS

Figure 1: LHn/B structure

(A). Ribbon diagram representation of LHn/B structure (Hn in blue, LC in cyan). Zinc ion is shown as an orange sphere.

(B). Superposition of LHn/B with BoNT/B (in grey, PDB code 1EPW, Swaminathan and Eswaramoorthy, 2000). Overall root mean square deviation was calculated with Swiss PDB viewer and was 0.95 Å for 837 C^{α}-atoms.

Figure 2: VAMP cleavage assay

(A). Enzymatic assay. Cleavage of VAMPs by LHn/B. Results were obtained by densitometry analysis and plotted. Non-linear fit was done with GraFit following Michaelis-Menten equation. Results for VAMP-1: *Km*= 12±3, *Vmax*= 157±12; VAMP-2: *Km*= 6.0±4.3, *Vmax*= 150±27; VAMP-3: *Km*= 3.2 ±1.4, *Vmax*= 27.9±3.5 (*Km* in μM, *Vmax* in pmol/hour/μg enzyme).

(B). CLUSTALW alignment (EBI) of human VAMP-1,-2 and -3. Regions important for VAMP-2 cleavage by BoNTs are coloured in grey (Chen et al., 2008; Sikorra et al., 2008), numbers correspond to VAMP-2 residues. The C-terminal transmembrane domain is indicated.

Figure 3: Spinal cord neuron assay

(A). Western blot analysis of VAMP-2 from cell lysates after treatment with decreasing concentrations of LHn/B and BoNT/B.

(B). Analysis of intracellular cleavage of VAMP-1 (circles and squares) and -2 (triangles and diamonds) after treatment with LHn/B and BoNT/B respectively. Results were obtained by densitometry analysis and plotted. Non-linear fit was done with GraFit.

REFERENCES

Agarwal R., Eswaramoorthy S., Kumaran D., Binz T. and Swaminathan S., 2004. Structural analysis of botulinum neurotoxin type E catalytic domain and its mutant Glu212-->Gln reveals the pivotal role of the Glu212 carboxylate in the catalytic pathway. *Biochemistry* 43, 6637–44

Agarwal R., Binz T. and Swaminathan S., 2005. Structural analysis of botulinum neurotoxin serotype F light chain: implications on substrate binding and inhibitor design. *Biochemistry* 44, 11758–11765

Agarwal R., Schmidt J.J., Stafford R.G. and Swaminathan S., 2009. Mode of VAMP substrate recognition and inhibition of Clostridium botulinum neurotoxin F. *Nat. Struct. Mol. Biol.* 16, 789–794

Arndt J.W., Yu W., Bi F. and Stevens R.C., 2005. Crystal structure of botulinum neurotoxin type G light chain: serotype divergence in substrate recognition. *Biochemistry* 44, 9574–9580

Arndt J.W., Chai Q., Christian T. and Stevens R.C., 2006. Structure of botulinum neurotoxin type D light chain at 1.65 A resolution: repercussions for VAMP-2 substrate specificity. *Biochemistry* 45, 3255–3262

Barnes M.P., Introduction to the clinical use of Botulinum neurotoxins, in: Foster K.A, Hambleton P. and Shone C.C. (2007) Treatments from toxins–the therapeutic potential of Clostridial neurotoxins, CRC press, Boca Raton, Florida, pp. 139–162.

Breidenbach M.A., and Brünger A.T., 2004. Substrate recognition strategy for botulinum neurotoxin serotype A. *Nature* 432**,** 925–929

Brünger A.T., Breidenbach M.A., Jin R., Fischer A., Santos J.S. and Montal M., 2007.

Botulinum neurotoxin heavy chain belt as an intramolecular chaperone for the light chain. *PLoS Pathog*. 3, 1191–1194

Chaddock J.A., Herbert M.H., Ling R.J., Alexander F.C.G., Fooks S.J., Revell D.F., Quinn C.P., Shone C.C. and Foster K.A., 2002. Expression and purification of catalytically active, non-toxic endopeptidase derivatives of Clostridium botulinum toxin type A. *Protein Expr. Purif.* 25, 219–228.

Chaddock J.A. and Marks P.M.H., 2006. Clostridial neurotoxins: structure-function led design of new therapeutics. *Cell. Mol. Life Sci.* 63, 540–551.

Chen S. and Barbieri J.T., 2007. Multiple pocket recognition of SNAP25 by botulinum neurotoxin serotype E. *J. Biol. Chem.* 282**,** 25540–25547

Chen S., Hall C. and Barbieri J.T., 2008. Substrate recognition of VAMP-2 by botulinum neurotoxin B and tetanus neurotoxin. *J. Biol. Chem*. 283, 21153–21159

Collaborative Computational Project, Number 4., 1994. The CCP4 suite: programs for protein crystallography. *Acta Crystallogr*. D50, 760–763.

Davis I.W., Leaver-Fay A., Chen V.B., Block J.N., Kapral G.J., Wang X., Murray L.W., Arendall W.B., Snoeyink J., Richardson J.S. and Richardson D.C., 2007. MolProbity: all-atom contacts and structure validation for proteins and nucleic acids. *Nucleic Acids Res.* 35, W375–W383

Emsley P., and Cowtan K., 2004. Coot: model-building tools for molecular graphics. *Acta Crystallogr*. D60, 2126–2132

Fischer A. and Montal M., 2007. Crucial role of the disulfide bridge between botulinum neurotoxin light and heavy chains in protease translocation across membranes. *J. Biol. Chem.* 282, 29604–29611

Fischer A., Mushrush D.J., Lacy D.B. and Montal M., 2008. Botulinum neurotoxin devoid

of receptor binding domain translocates active protease. *PLoS Pathog.* 4, e1000245

Foster K.A., 2009. Engineered toxins: new therapeutics. *Toxicon* 54, 587–592.

Galloux M., Vitrac H., Montagner C., Raffestin S., Popoff M.R., Chenal A., Forge V. and Gillet D., 2008. Membrane interaction of botulinum neurotoxin A T domain: The belt region is a regulatory loop for membrane interaction. *J. Biol. Chem*. 283, 27668–27676

Jin R., Sikorra S., Stegmann C.M., Pich A., Binz T. and Brünger A.T., 2007. Structural and biochemical studies of botulinum neurotoxin serotype C1 light chain protease: implications for dual substrate specificity. *Biochemistry* 46, 10685–10693

Koriazova L.K. and Montal M., 2003. Translocation of botulinum neurotoxin light chain protease through the heavy chain channel. *Nat. Struct. Biol.* 10, 13–18

Kumaran D., Eswaramoorthy S., Furey W., Navaza J., Sax M. and Swaminathan S., 2009. Domain organization in Clostridium botulinum neurotoxin type E is unique: its implication in faster translocation. *J. Mol. Biol.* 386, 233–245

Lacy D.B., Tepp W., Cohen A.C., DasGupta B.R., and Stevens R.C., 1998. Crystal structure of botulinum neurotoxin type A and implications for toxicity. *Nat. Struct. Biol.* 5, 898–902

Lacy D.B., and Stevens R.C., 1999. Sequence homology and structural analysis of the clostridial neurotoxins. *J. Mol. Biol.* 291, 1091–1104

Leslie A.G.W., 2006. The integration of macromolecular diffraction data. *Acta Crystallogr*. D62, 48-57.

Masuyer G., Thiyagarajan N., James P.L., Marks P.M., Chaddock J.A. and Acharya K.R., 2009. Crystal structure of a catalytically active, non-toxic endopeptidase derivative of Clostridium botulinum toxin A. *Biochem. Biophys. Res. Commun.* 381, 50–53

McCoy J.A., Grosse-Kunstleve R.W., Adams P.D., Winn M.D., Storoni L.C. and Read R.J., 2007. Phaser crystallographic software. *J. Appl. Crystllogr.* 40, 658–674

McMahon H.T., Ushkaryov Y.A., Edelmann L., Link E., Binz T., Niemann H., Jahn J. and Südhof T.C., 1993. Cellubrevin is a ubiquitous tetanus-toxin substrate homologous to a putative synaptic vesicle fusion protein. *Nature* 364, 346–349

Moore A.P., Expanding clinical uses of Botulinum neurotoxins, in: Foster K.A, Hambleton P. and Shone C.C. (2007) Treatments from toxins–the therapeutic potential of Clostridial neurotoxins, CRC press, Boca Raton, Florida, 2007, pp. 163–194

Proux-Gillardeaux V., Gavard J., Irinopoulou T., Mege R.M. and Galli T., 2005. Tetanus neurotoxin-mediated cleavage of cellubrevin impairs epithelial cell migration and integrin-dependent cell adhesion. *Proc. Natl. Acad. Sci. USA* 102, 6362–6367

Segelke B., Knapp M., Kadkhodayan S., Balhorn R. and Rupp B., 2004. Crystal structure of Clostridium botulinum neurotoxin protease in a product-bound state: Evidence for noncanonical zinc protease activity. *Proc. Natl. Acad. Sci. USA* 101, 6888–6893

Shone C.C., Hambleton P., and Melling J., 1985. Inactivation of Clostridium botulinum type A neurotoxin by trypsin and purification of two tryptic fragments. Proteolytic action near the COOH-terminus of the heavy subunit destroys toxin-binding activity. *Eur. J. Biochem.* 151, 75–82.

Sikorra S., Henke T., Galli T. and Binz T., 2008. Substrate recognition mechanism of VAMP/synaptobrevin-cleaving clostridial neurotoxins. *J. Biol. Chem.* 283, 21145–21152

Sudhof T.C. and Rothman J.E., 2009. Membrane fusion: grappling with SNARE and SM proteins. *Science* 323, 474–477

Swaminathan S. and Eswaramoorthy S., 2000. Structural analysis of the catalytic and

binding sites of Clostridium botulinum neurotoxin B. *Nat. Struct. Biol.* 7, 693–699

Takamori S., Holt M., Stenius K., Lemke E.A., Grønborg M., Riedel D., Urlaub H., Schenck S., Brügger B., Ringler P., Müller S.A., Rammner B., Gräter F., Hub J.S., De Groot B.L., Mieskes G., Moriyama Y., Klingauf J., Grubmüller H., Heuser J., Wieland F. and Jahn R., 2006. Molecular anatomy of a trafficking organelle. *Cell* 127, 831–846

Vagin A.A., Steiner R.S., Lebedev A.A., Potterton L., McNicholas S., Long F. and Murshudov G.N., 2004. REFMAC5 dictionary: organization of prior chemical knowledge and guidelines for its use. *Acta Crystallogr*. D60, 2184–2195

Table 1. X-ray data collection and refinement statistics

A. Data collection statistics	
Space group	$P2_12_12$
Number of molecules/asymmetric unit	1
Cell dimensions	a = 66.9, b =113.5, c =149.1Å
Resolution range (Å)	50-2.8
R_{symm}[a] (%)	12.1 (51.4)
I/σI (outer shell)	10.3 (3.5)
Completeness (outer shell) %	99.8 (100.0)
Total no. of reflections	165,586
Unique no. of reflections	28,644
Redundancy	5.8 (5.8)
Wilson B-factor ($Å^2$)	57.6
B. Refinement statistics	
Resolution range (Å)	50-2.8
R_{cryst}[b] (%)	24.0
R_{free}[c] (%)	28.2
Number of non-H atoms	
Protein	6828
Metal	1 zinc ion
Water molecules	31
Average temperature factor (B-factor) ($Å^2$)	Protein atoms- Chain A = 32.6, B = 40.8 (water molucules = 22.1)
RMSD in bond lengths (Å)	0.006
RMSD in bond angles (°)	0.86

[a] $R_{symm} = \Sigma_h \Sigma_i |I(h) - I_i(h)| / \Sigma_h \Sigma_i I_i(h)$, where $I_i(h)$ and I(h) are the i^{th} and the mean measurements of the intensity of reflection h, respectively.

[b] $R_{cryst} = \Sigma_h ||F_o| - |F_c|| / \Sigma_h F_o$, where F_o and F_c are the observed and calculated structure factor amplitudes of reflection h, respectively.

[c] R_{free} is equal to R_{cryst} for a randomly selected 5.0% subset of reflections not used in the refinement.

Figure 1: LHn/B structure

A **B**

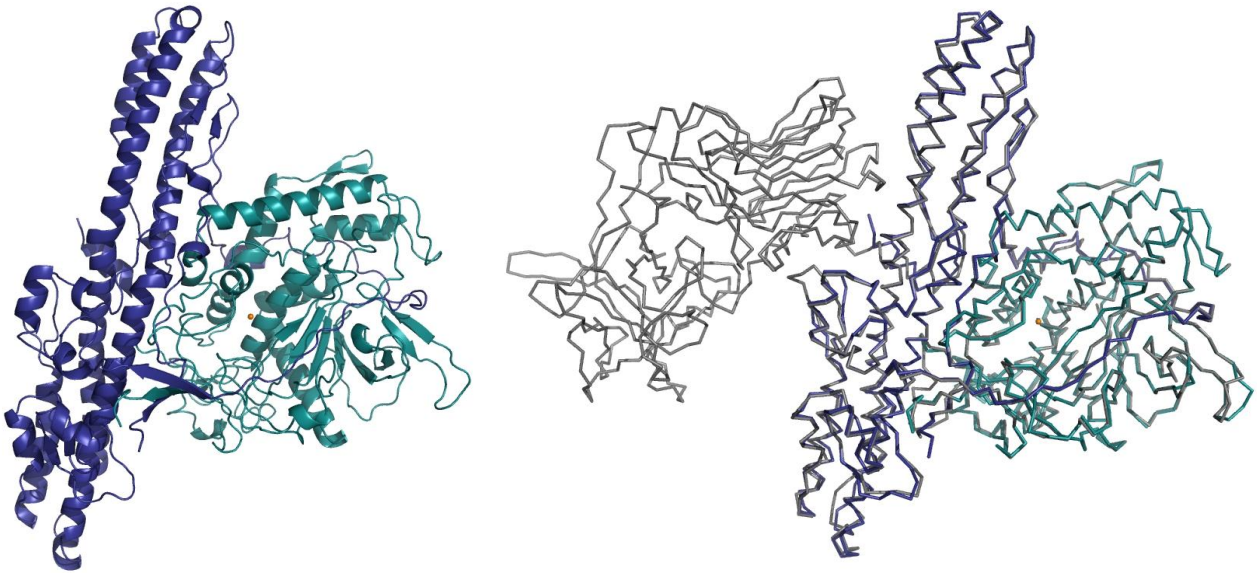

Figure 2: VAMP cleavage assay

A

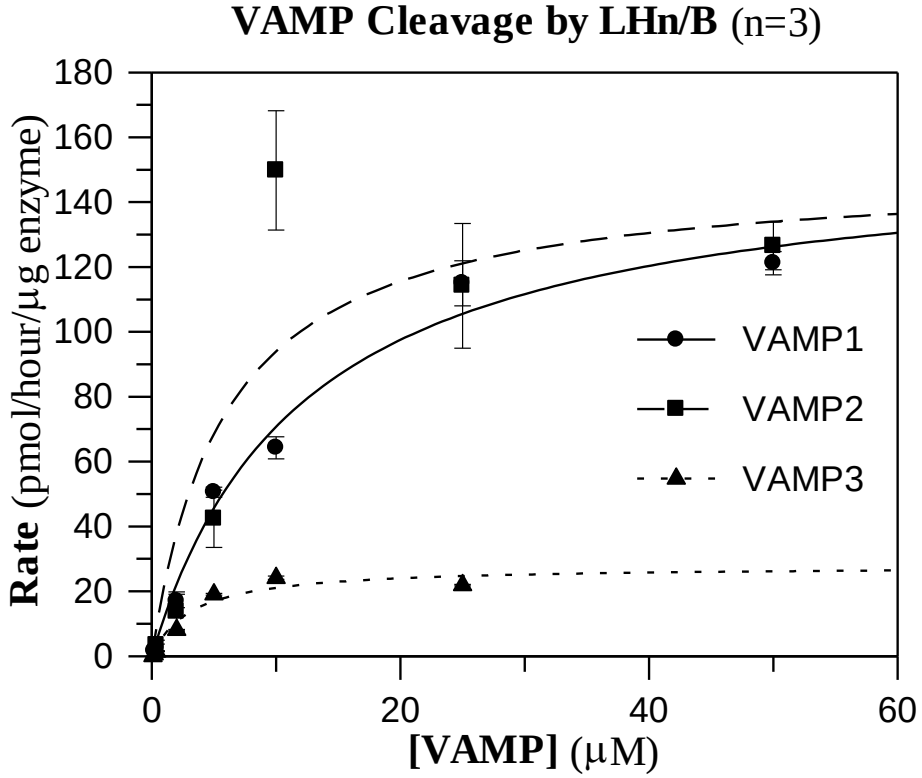

B

```
                                        20                  40
VAMP1_HUMAN     -MSAPAQPPAEGTEGTAPGGGPPGPPPNMTSNRRLQQTQAQVEEVVDIIRVNVDKVLERD
VAMP2_HUMAN     SATAATAPPAA----PAGEGGPPAPPPNLTSNRRLQQTQAQVDEVVDIMRVNVDKVLERD
VAMP3_HUMAN     ----STGPTAA----TG-------------SNRRLQQTQNQVDEVVDIMRVNVDKVLERD
                    .: *.*     ..               ********* **:*****:**********

                60                  80                  100
VAMP1_HUMAN     QKLSELDDRADALQAGASQFESSAAKLKRKYWWKNCKMMIMLGAICAIIVVVIVIYFFT-
VAMP2_HUMAN     QKLSELDDRADALQAGASQFETSAAKLKRKYWWKNLKMMIILGVICAIILIIIVYFSS-
VAMP3_HUMAN     QKLSELDDRADALQAGASQFETSAAKLKRKYWWKNCKMWAIGITVLVIFIIIIVWVVSS
                **********************:********** **  :  .: .*::::*:::. :
                                                    TM
```

Figure 3: Spinal cord neuron assay

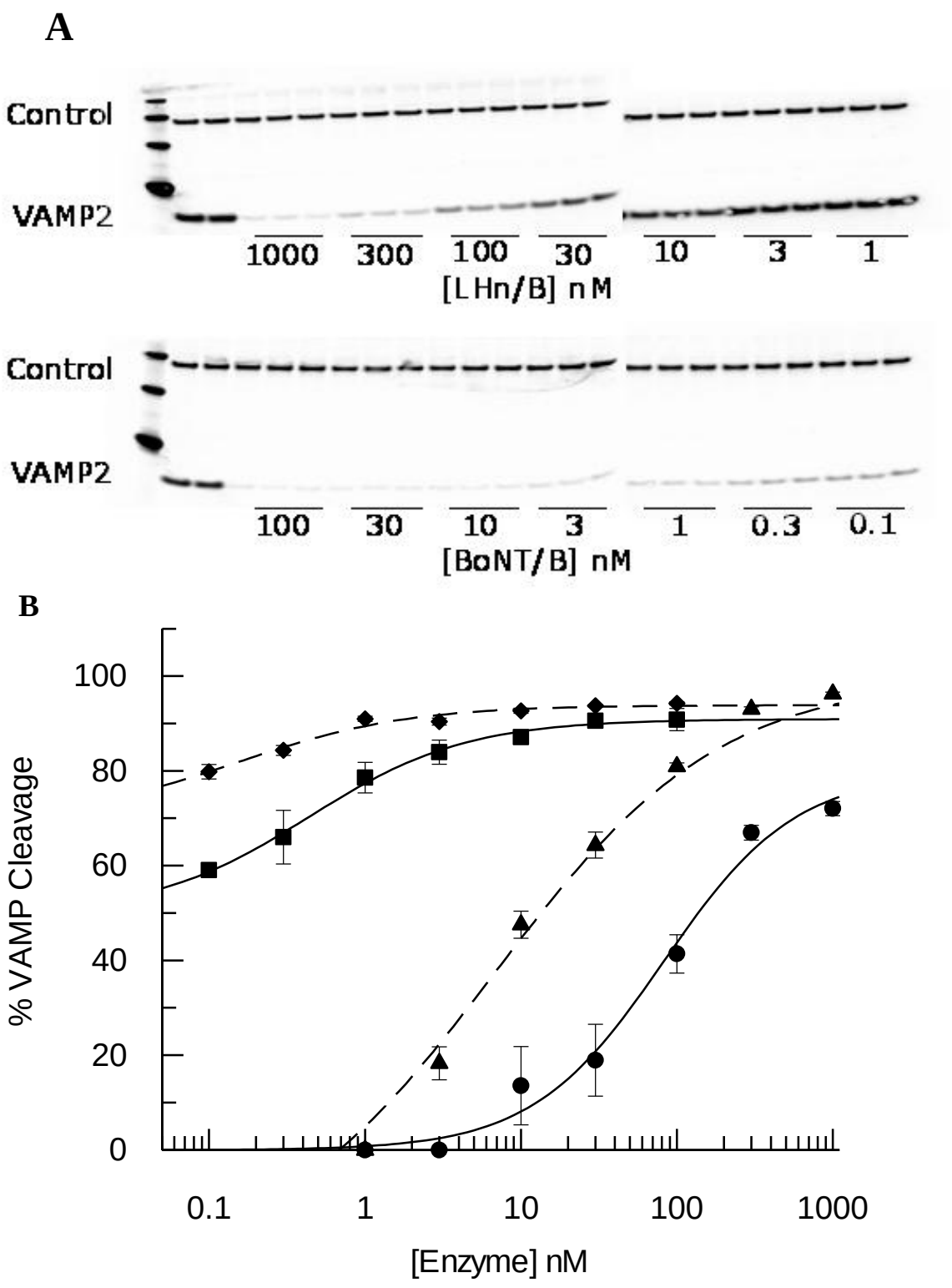

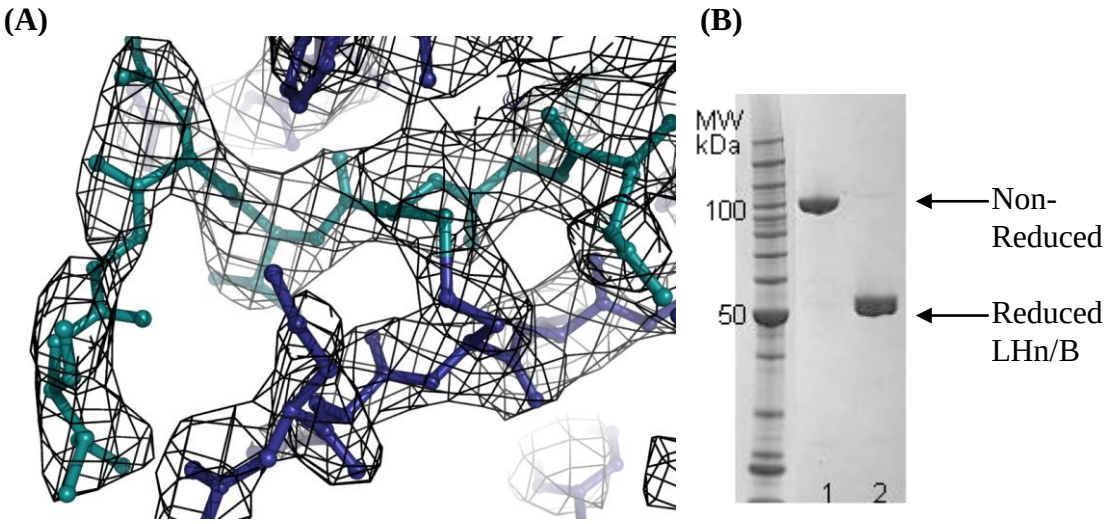

Fig. S1. (a) Structure of LHn/B: LC (Cyan)-Hn (Blue) interaction at the disulphide bridge – Factor Xa cleavage site for activation. 2|Fo|-|Fc| map at 1σ.
(b) SDS-PAGE of purified LHn/B under non-reducing (1) and reducing conditions (2).

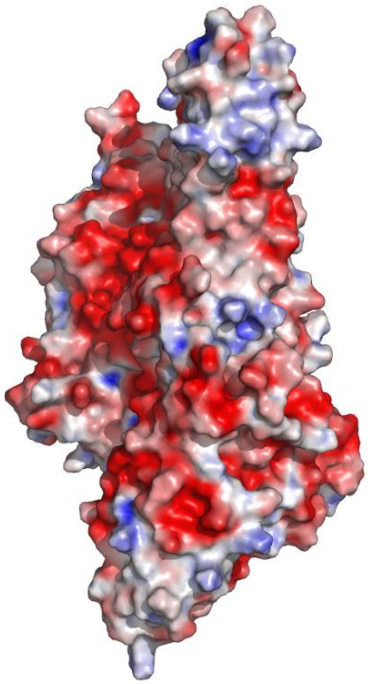

Fig. S2. Structure of LHn/B: newly accessible solvent surface. Electrostatic potential calculated using APBS in PyMOL (Negative potential in red, Positive in blue).